PERGAMON

International Journal of Heat and Mass Transfer 43 (2000) 4299–4310

International Journal of HEAT and MASS TRANSFER

www.elsevier.com/locate/ijhmt

# Heat transfer optimization in corrugated wall channels

Giampietro Fabbri

*Dipartimento di Ingegneria Energetica, Nucleare e del Controllo Ambientale, Universitá degli studi di Bologna, Via Zannoni 45/2, 40134 Bologna, Italy*

Received 23 June 1999; received in revised form 27 January 2000

**Abstract**

In this work, the heat transfer in a channel composed of a smooth and a corrugated wall is studied under laminar flow conditions. The velocity and temperature distributions are determined with the help of a finite element model. The heat transfer performance of the corrugated wall channel is compared with that of a smooth wall duct. The numerical model is utilized in a genetic algorithm to maximize the heat transfer by optimizing the corrugation profile, for given volume of the corrugated wall and pressure drop in the channel. Some optimum corrugation profiles are presented at the end. © 2000 Elsevier Science Ltd. All rights reserved.

*Keywords:* Forced convection; Heat transfer; Optimization

## 1. Introduction

The fluid dynamical and thermal phenomena occurring in corrugated wall channels have been studied in different engineering sectors. Corrugated surfaces are, for example, utilized in compact heat exchangers [1]. The corrugation allows the heat transfer surface between dissipators and coolant fluids to be extended, maintaining at the same time a reduced dissipator volume and weight. The study of the heat transfer through corrugated surface is also particularly interesting for the applications in the electronic industry [2,3]. In fact, the cooling of electronic devices is often carried out by forcing a fluid flow on the boards where the devices are soldered. Due to the presence of the devices and, in some cases, dissipators, the profile of the board surface can be schematized with more or less continuous and regular corrugations.

Many theoretical and experimental studies are available in the literature on the fluid dynamical and thermal phenomena occurring in corrugated wall channels [4–13]. Various heat transfer characteristics have been observed under different conditions. In general, the corrugation of the walls extends the heat transfer surface of the channels and generates turbulence even at low Reynolds numbers. If the eddy velocity is sufficiently high and the fluid is not very conductive, the turbulent phenomena can enhance the local convection coefficient. However, the pressure drop in corrugated wall channels is higher than in flat wall channels of the same external size. Moreover, the corrugation of the walls, in some cases, can induce stagnation of the coolant fluid. As a consequence, the local convection coefficient is so reduced that, even if the heat transfer surface between the wall and the fluid is extended, the global heat transfer effectiveness does not overcome that of a flat wall channel of a comparable size. Therefore, the heat transfer effectiveness of corrugated channel depends on many

*E-mail address:* giampietro.fabbri@mail.ing.unibo.it (G. Fabbri).


PII: S0017-9310(00)00054-5

**Nomenclature**

| | |
|---|---|
| $c$ | specific heat capacity of the fluid (J/kg K) |
| $d$ | distance between the external surfaces of the channel (m) |
| $f$ | corrugated wall thickness (m) |
| $F$ | normalized corrugated wall thickness |
| $\bar{F}$ | average normalized corrugated wall thickness |
| $h_x$ | local heat transfer coefficient (W/m$^2$ K) |
| $k_f$, $k_s$ | thermal conductivity of the fluid and solid (W/m K) |
| $l$ | period of the corrugation function (m) |
| $L$ | normalized period of the corrugation function |
| $Nu_e$ | equivalent Nusselt number |
| $Nu_x$ | local equivalent Nusselt number |
| $p$ | sum of the pressure and the gravity potential contribution (Pa) |
| $P$ | normalized pressure |
| $Pr$ | Prandtl number |
| $q''$ | heat flux per unit of surface (W/m$^2$) |
| $Re$ | Reynolds number |
| $t_f$, $t_s$ | temperature of the fluid and solid (K) |
| $T_f$, $T_s$ | normalized temperature of the fluid and solid |
| $t_{b0}$ | bulk temperature in the reference channel (K) |
| $T_{b0}$ | normalized bulk temperature in the reference channel |
| $u$, $v$ | velocity components in the $x$- and $y$-directions (m/s) |
| $U$, $V$ | normalized velocity components |
| $w$ | average velocity in the corrugated channel (m/s) |
| $w_0$ | average velocity in the reference channel (m/s) |
| $x$, $y$ | longitudinal and transversal coordinates |
| $X$, $Y$ | normalized coordinates |

*Greek symbols*

| | |
|---|---|
| $\alpha$ | convergence parameter |
| $\gamma$ | ratio between solid and fluid thermal conductivity |
| $\Delta p_0$ | pressure drop in the reference channel for a length equal to $l$ (Pa) |
| $\Delta P$ | normalized pressure drop for a length equal to $l$ (Pa) |
| $\mu$ | dynamic viscosity of the fluid (kg/m s) |
| $\rho$ | density of the fluid (kg/m$^3$) |

factors concerning the geometry of the walls, the properties of the coolant fluid, and the nature of the flow. Moreover, it can only be correctly compared with the heat transfer effectiveness of flat wall channels by also considering the external size, the wall volume or weight and the pressure drop.

Most of the studies performed on the fluid dynamical and thermal phenomena occurring in corrugated wall channels consider corrugations having a periodical pattern which is described by simple functions such as rectangular, triangular, or sinusoidal. However, due to the variety of thermal and fluid dynamical characteristics described in the literature under different conditions, the study of more complex corrugation profiles can be useful to better evaluate the convenience of assigning to the channel walls corrugated rather than flat profiles.

In the present work, the problem of optimizing the heat transfer is studied in a channel composed of a flat insulated wall and a corrugated one crossed by a heat flux uniformly imposed. The analysis is limited to the region where the dynamic and thermal profile is fully developed, under laminar flow conditions. To the corrugated wall profile, a periodical pattern is assigned, which is described by a fifth order polynomial function. The velocity and temperature distributions are determined with the help of a finite element model. The performance of the corrugated wall channel is compared with that of a conduit composed of two zero thickness flat walls having the same external size. Moreover, the finite element model is utilized in an original genetic algorithm to determine the values of the polynomial profile parameters which optimize the heat transfer performance of the corrugated channel for given volume of the wall or pressure drop in the channel. Finally, some optimum corrugation profiles are presented for different situation.

## 2. The mathematical model

Let us consider a channel composed of two parallel flat walls. One wall is smooth and thermally insulated, and the other is corrugated and crossed by a heat flux $q''$ which is uniformly imposed on its external surface (Fig. 1). Moreover, the thickness of the insulated wall is ideally zero, while that of the corrugated wall is a periodical function $f$ of the longitudinal coordinate $x$, whose period is $l$. Between the two walls, a coolant fluid passes through in laminar flow in the $x$ direction.

Let us introduce the following hypotheses:

- the system is in steady state;

- the velocity and temperature profiles are fully developed;
- the fluid properties are uniform;
- the viscous dissipation within the fluid is negligible.

Let $y$ be the transversal coordinate. Due to the symmetry in the normal to plane $(x, y)$ direction, the heat transfer performances of the channel can be studied by only determining the velocity and temperature distributions on the plane $(x, y)$. Moreover, due to the periodicity of the channel shape, the study can be limited to a portion whose length is equal to $l$.

The velocity distribution must satisfy the force and mass balance equations, which for a steady-state incompressible flow can be reduced to the following form:

$$\rho\left(\frac{\partial u^2}{\partial x}+\frac{\partial uv}{\partial y}\right)=-\frac{\partial p}{\partial x}+\mu\left(\frac{\partial^2 u}{\partial x^2}+\frac{\partial^2 u}{\partial y^2}\right) \tag{1}$$

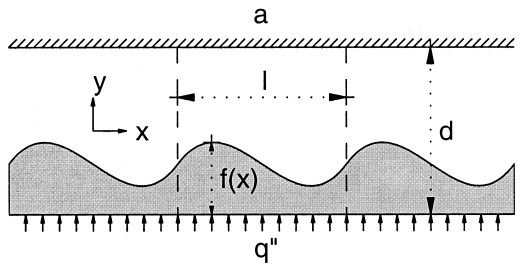


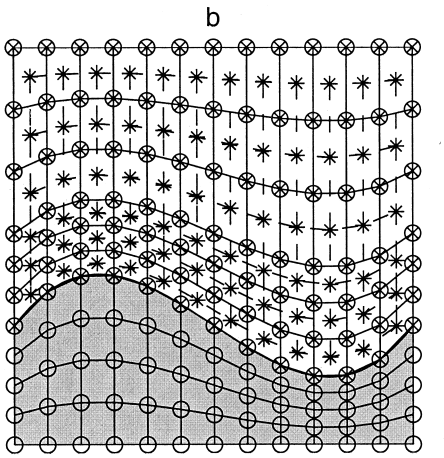


Fig. 1. (a) Corrugated channel. (b) Grids of the temperature (○), pressure (×), and velocity (∗).

$$\rho\left(\frac{\partial vu}{\partial x}+\frac{\partial v^2}{\partial y}\right)=-\frac{\partial p}{\partial y}+\mu\left(\frac{\partial^2 v}{\partial x^2}+\frac{\partial^2 v}{\partial y^2}\right) \tag{2}$$

$$\frac{\partial u}{\partial x}+\frac{\partial v}{\partial y}=0 \tag{3}$$

where $\rho$ and $\mu$ are the density and the dynamic viscosity of the fluid, respectively, $u$ and $v$ are the velocity components in the $x$- and $y$- direction, respectively, and $p$ is the sum of the pressure and the gravity potential contribution.

The temperature distributions in both the fluid and the solid must satisfy the following energy balance equation:

$$\rho c\left(\frac{\partial t_f u}{\partial x}+\frac{\partial t_f v}{\partial y}\right)=k\left(\frac{\partial^2 t_f}{\partial x^2}+\frac{\partial^2 t_f}{\partial y^2}\right) \tag{4}$$

$$\frac{\partial^2 t_s}{\partial x^2}+\frac{\partial^2 t_s}{\partial y^2}=0 \tag{5}$$

$c$ and $k$ being the specific heat and the thermal conductivity of the fluid, respectively, and $t_f$ and $t_s$ the temperature in the fluid and in the solid, respectively.

Eqs. (1)–(5) can be reduced to a dimensionless form by introducing a reference channel delimited by an insulated flat surface and a flat surface crossed by a uniform heat flux equal to $q''$. Let the reference channel surfaces be at the same distance $d$ as the corrugated channel external surfaces. Moreover, assuming in the reference channel the same flow rate of the same fluid as in the corrugated one, let $w_0$ be the average velocity and $\Delta p_0$ the pressure drop in a portion of the reference channel whose length is equal to $l$. The following dimensionless entities can now be introduced:

$$\begin{gathered} X=\frac{x}{d}\quad Y=\frac{y}{d}\quad L=\frac{l}{d}\quad F(X)=\frac{f(Xd)}{d}\quad U=\frac{u}{w_0} \\ V=\frac{v}{w_0}\quad P=\frac{p}{\Delta p_0}\quad T_f=\frac{t_f}{\Delta t}\quad T_s=\frac{t_s}{\Delta t} \end{gathered} \tag{6}$$

where $\Delta t$ is the coolant fluid bulk temperature drop which is the same in the reference and corrugate channel portion. By substituting the dimensionless entities in Eqs. (1)–(5), the following dimensionless equations are obtained:

$$\frac{\partial U^2}{\partial X}+\frac{\partial UV}{\partial Y}=-\frac{24L}{Re}\frac{\partial P}{\partial X}+\frac{2}{Re}\left(\frac{\partial^2 U}{\partial X^2}+\frac{\partial^2 U}{\partial Y^2}\right) \tag{7}$$

$$\frac{\partial VU}{\partial X}+\frac{\partial V^2}{\partial Y}=-\frac{24L}{Re}\frac{\partial P}{\partial Y}+\frac{2}{Re}\left(\frac{\partial^2 V}{\partial X^2}+\frac{\partial^2 V}{\partial Y^2}\right) \tag{8}$$

$$\frac{\partial U}{\partial X}+\frac{\partial V}{\partial Y}=0 \tag{9}$$

$$\frac{\partial T_f U}{\partial X}+\frac{\partial T_f V}{\partial Y}=\frac{2\gamma}{RePr}\left(\frac{\partial^2 T_f}{\partial X^2}+\frac{\partial^2 T_f}{\partial Y^2}\right) \tag{10}$$

$$\frac{\partial^2 T_s}{\partial X^2}+\frac{\partial^2 T_s}{\partial Y^2}=0 \tag{11}$$

where $Re=\rho w(x)2[d-f(x)]/\mu=\rho w_0 2d/\mu$ and $Pr=\mu c/k_f$ are the Reynolds and Prandtl numbers, respectively, and are the same for the corrugated and the reference channel.

Eqs. (7)–(9) must be integrated by imposing the following boundary conditions:

$$U(X,1)=V(X,1)=U\big(X,F(X)\big)=V\big(X,F(X)\big)=0 \tag{12}$$

$$U(0,Y)=U(L,Y) \tag{13}$$

$$V(0,Y)=V(L,Y) \tag{14}$$

$$P(0,Y)=P(L,Y)+\Delta P \tag{15}$$

$$\left.\frac{\partial V}{\partial X}\right|_{(0,Y)}=\left.\frac{\partial V}{\partial X}\right|_{(L,Y)} \tag{16}$$

$\Delta P$ being the normalized pressure drop between the inlet and the outlet section of the corrugated channel portion. Moreover, the value of the pressure in one point of the channel is required.

Eqs. (10) and (11) must be integrated by imposing that temperatures and heat fluxes in the normal to the surface direction are identical in the solid and in the fluid on the contact surface, and:

$$T_f(L,Y)=T_f(0,Y)+1 \tag{17}$$

$$T_s(L,Y)=T_s(0,Y)+1 \tag{18}$$

$$\left.\frac{\partial T_f}{\partial X}\right|_{(0,Y)}=\left.\frac{\partial T_f}{\partial X}\right|_{(L,Y)} \tag{19}$$

$$\left.\frac{\partial T_s}{\partial X}\right|_{(0,Y)}=\left.\frac{\partial T_s}{\partial X}\right|_{(L,Y)} \tag{20}$$

$$\left.\frac{\partial T_f}{\partial Y}\right|_{(X,1)}=0 \tag{21}$$

$$\left.\frac{\partial T_s}{\partial Y}\right|_{(X,0)}=-\frac{1}{2\gamma}RePr \tag{22}$$

where $\gamma$ is the ratio between the thermal conductivity of the solid and that of the fluid. Moreover, the value of the temperature in one point of the channel is required.

Velocity, pressure and temperature distributions in the corrugated channel portion can be numerically determined by utilizing a finite element method like the following one. In the channel portion, two staggered grids can be drawn as in Fig. 2. In the nodal points, discrete distributions are considered for velocity, pressure, or temperature. In the trapezoidal elements delimited between four adjacent nodes, the generic continuous entity $E$ (velocity, pressure, or temperature) can be approximated by an interpolation of the values $E_k$ which it assumes in the four nodes:

$$E=\sum_k \frac{X-X_{j(k)}}{X_k-X_{j(k)}}\frac{Y-a_{i(k)}-b_{i(k)}X}{a_k-a_{i(k)}+\big(b_k-b_{i(k)}\big)X}E_k \tag{23}$$

where $X_k$ and $X_{j(k)}$ are node coordinates in the longitudinal direction, $a_k+b_kX$ is the value which $Y$ assumes on the line passing through the oblique side where node $k$ is, and $a_{i(k)}+b_{i(k)}X$ is the value which $Y$ assumes on the opposite side. In this way, $E$ linearly changes on the element sides and on the segments joining the middle points of each couple of opposite sides.

Eqs. (7)–(11) can now be integrated after having divided each trapezoidal element in four subelements by joining the middle points of the opposite sides. For each node where $U$, $V$, or $P$ is unknown, Eqs. (7)–(9), respectively, must be integrated on the four subelements surrounding the node. By taking boundary conditions (12)–(16) into account, the following system of equations are obtained:

$$\Big[A+B_x*\mathrm{diag}(\bar{U})+B_y*\mathrm{diag}(\bar{V})\Big]*\bar{U}+S_x*\bar{P}+M_x*\Delta P=N_x*P_n \tag{24}$$

$$\Big[A+B_x*\mathrm{diag}(\bar{U})+B_y*\mathrm{diag}(\bar{V})\Big]*\bar{V}+S_y\bar{P}+M_y*\Delta P=N_y*P_n \tag{25}$$

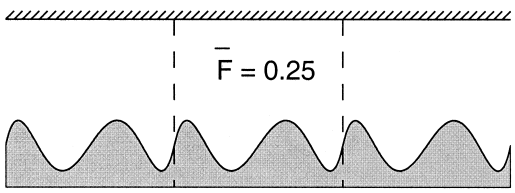


Fig. 2. Optimum channel geometry for $Re$ = 500 and $Pr$ = 5.

$$C_x \times \bar{U} + C_y \times \bar{V} = 0 \tag{26}$$

where the operator diag transforms the argument vector in a diagonal matrix, vectors $\bar{U}$ and $\bar{V}$ contain the velocity components of all points of the velocity grid, and vector $\bar{P}$ contains the pressure values in all points of the pressure grid with the exception of those on the outlet section and that where the pressure is known and equal to $P_n$. Moreover, matrix $A$ introduces the contribution of the momentum diffusion, while matrices $B_x$ and $B_y$ of the momentum convection in the $x$- and $y$- direction, respectively. Finally, matrices $C_x$ and $C_y$ introduce the contribution of the mass transfer into account in the $x$- and $y$-directions, respectively.

Systems (24)–(26) provide as many equations as the unknown values of $U$, $V$, and $P$, respectively. Since $\Delta P$ is unknown, while the volume flow rate per unit of width $\dot{V}'$ in the corrugated and reference channel is the same, the following equation can be added:

$$D * \bar{U} = \dot{V}' = 1 \tag{27}$$

By solving the system composed of systems (24)–(27), the normalized pressure drop in the channel and the discrete distributions of the velocity and pressure can be determined. An arbitrary value can be assigned to $P_n$, since it does not influence the pressure drop neither the velocity distribution, which only are important to evaluate the heat transfer performances of the corrugated channel. Since the system is not linear, it can be solved iteratively. To linearize systems (24) and (25), the arguments $\bar{U}$ and $\bar{V}$ of the operator diag can be replaced by vectors $\bar{U}_a$ and $\bar{V}_a$, respectively, which contains arbitrary known values of the velocity components. After solution of the linearized global system, vectors $\bar{U}_a$ and $\bar{V}_a$ can be updated in the following way:

$$\bar{U}_a = (1-\alpha) \times \bar{U}_a + \alpha \times \bar{U} \tag{28}$$

$$\bar{V}_a = (1-\alpha) \times \bar{V}_a + \alpha \times \bar{V} \tag{29}$$

where $\alpha$ is a parameter ranging from 0 to 1. The procedure can be iterated until relative changes in vectors $\bar{U}_a$ and $\bar{V}_a$ become smaller than an established value.

After having determined the discrete velocity distribution, Eqs. (10) and (11) can be integrated on the surface of the four subelements surrounding each node of the temperature grid where values are unknown. By taking boundary conditions (17)–(22) into account, the following system of equations is obtained:

$$\left[H + G_x * \mathrm{diag}\left(\bar{U}_t\right) + G_y * \mathrm{diag}\left(\bar{V}_t\right)\right] \times \bar{T} = M_t + N_t * T_n \tag{30}$$

where $\bar{T}$ contains the temperature values in all points of the temperature grid with the exception of those on the outlet section and that where temperature is known and equal to $T_n$, and vectors $\bar{U}_t$ and $\bar{V}_t$ contain the velocity component values calculated in the same points. Moreover, matrix $H$ introduces the contribution of the conduction, while matrices $G_x$ and $G_y$ the convection in the $x$- and $y$-directions, respectively. Lastly, vector $M_t$ takes the temperature drop between the outlet and the inlet section into account, which is, after normalization, equal to 1.

By solving the system (30), the discrete temperature distributions is determined as a function of $T_n$, which can be arbitrarily assigned. Due to the linearity of the system, in fact, the heat transfer performances of the channel are not determined by the value of $T_n$.

To compare the heat transfer performances of the corrugated channel with those of the reference one, let us suppose that the inlet bulk temperature is the same for both channels. Under this condition, let $t_{b0}(x)$ be the bulk temperature which occurs in the reference channel. Now, let us suppose that the temperature distribution on the external surface of the corrugated wall occurred on the corresponding surface of the reference channel. In this case, the local heat transfer coefficient in the reference channel would be:

$$h_x = \frac{q''}{t_s(x,0) - t_{b0}(x)} \tag{31}$$

The local Nusselt number would then result:

$$Nu_x = \frac{h_x 2d}{k} \tag{32}$$

Referring to the dimensionless entities, $Nu_x$ can be calculated as follows:

$$Nu_x = \frac{RePr}{L} \frac{1}{T_s(X,0) - T_{b0}(X)} \tag{33}$$

An equivalent Nusselt number for the corrugated channel can then be defined as the average of $Nu_x$:

$$Nu_e = \frac{1}{L} \int_0^L Nu_x \, dX \tag{34}$$

Such an equivalent Nusselt number corresponds to the average Nusselt number which would be calculated for the reference channel if on its heat flux crossed surface occurred the same temperature distribution as on the corrugated channel, for given heat flux and inlet bulk temperature. It depends on the channel geometry, $Re$, $Pr$, and $\gamma$.

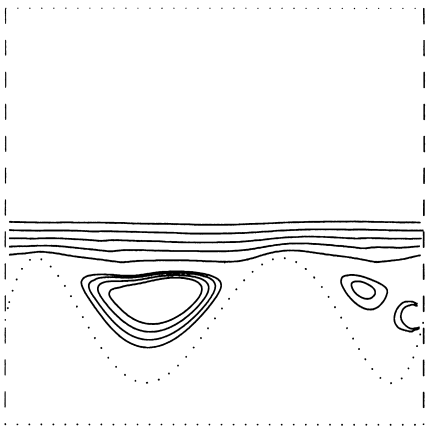

Fig. 3. Streamlines near the corrugated wall of Fig. 2 for $Re = 500$.

## 3. Results

The mathematical model described in Section 2 has been utilized in a genetic algorithm [14–18] to determine the corrugation profile which provide the best heat transfer performance under different conditions.

To the pressure and temperature grids, $25 \times 50$ and $30 \times 50$ nodes have been assigned, respectively. As a consequence, $24 \times 49$ nodes have been assigned to the velocity grid. More close grids have been tested without finding any significant variation in $Nu_e$ or in $\Delta P$. In the testing cases, a pressure grid of $31 \times 50$ elements produced alterations in $Nu_e$ and $\Delta P$ of 0.3% and 0.25%. The same alterations were produced by a pressure grid of $25 \times 60$ elements. In the cases where $F(X)$ was constant, the velocity and the temperature distributions obtained with the model with the selected grid were in good agreement with the analytical one-dimensional solution and the numerical errors in $Nu_e$ and $\Delta P$ were less than 0.13% and 0.12%, respectively.

For the corrugation profile function $F(X)$, a fifth order polynomial form has been assumed. In this way, two waves can be obtained in the corrugation profile. Moreover, by imposing that the function and its first derivative assume the same value in $X = 0$ and $X = L$, the corrugation profile is univocally determined by four points. Therefore, as corrugation profile describing parameters the values $F_i$ assumed by $F(X)$ in the first four of six equidistant points between 0 and $L$ have been assumed.

In the genetic algorithm, 12 sample populations and 33% selection percentage have been established. During parameter reproduction, random errors uniformly distributed between $-10$ and $+10$% of the parameter values were introduced. The parameter set was composed of the corrugation parameters $F_i$ and parameter $\alpha$. To each sample the value of the equivalent Nusselt number was assigned. However, if the velocity distribution was not found within an established num-

Table 1
Characteristic parameters of the wall corrugations which maximize $Nu_e$ under different conditions

| Constraint | $Re$ | $Pr$ | $F_0$ | $F_1$ | $F_2$ | $F_3$ | $\bar{F}$ | $Nu_e$ | $\Delta P$ |
|---|---|---|---|---|---|---|---|---|---|
| – | 100 | 1 | | | | | | 8.94 | 4.63 |
| – | 100 | 5 | 0.4 | 0.4 | 0.4 | 0.4 | 0.4 | 8.94 | 4.63 |
| – | 500 | 1 | | | | | | 8.94 | 4.63 |
| – | 500 | 5 | 0.25 | 0.234 | 0.128 | 0.372 | 0.25 | 9.62 | 4.18 |
| $\bar{F}$ | 100 | 1 | | | | | | 6.91 | 3.52 |
| $\bar{F}$ | 100 | 5 | 0.263 | 0.269 | 0.101 | 0.207 | 0.2 | 7.24 | 3.52 |
| $\bar{F}$ | 500 | 1 | | | | | | 7.32 | 3.9 |
| $\bar{F}$ | 500 | 5 | | | | | | 8.77 | 3.9 |
| $\Delta P$ | 100 | 1 | | | | | | 7.29 | 2.5 |
| $\Delta P$ | 100 | 5 | 0.263 | 0.263 | 0.263 | 0.263 | 0.263 | 7.29 | 2.5 |
| $\Delta P$ | 500 | 1 | | | | | | 7.29 | 2.5 |
| $\Delta P$ | 500 | 5 | 0.193 | 0.184 | 0.117 | 0.269 | 0.193 | 7.34 | 2.5 |
| $\Delta P$ | 100 | 1 | | | | | | 7.75 | 3 |
| $\Delta P$ | 100 | 5 | 0.307 | 0.307 | 0.307 | 0.307 | 0.307 | 7.75 | 3 |
| $\Delta P$ | 500 | 1 | | | | | | 7.75 | 3 |
| $\Delta P$ | 500 | 5 | 0.215 | 0.203 | 0.121 | 0.309 | 0.215 | 8.08 | 3 |

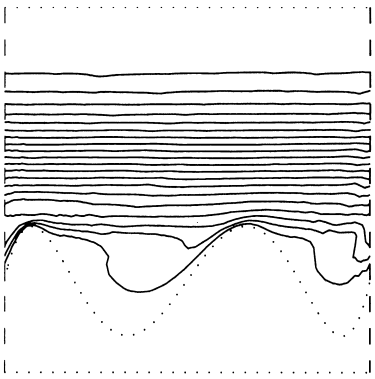

Fig. 4. Isothermal curves in the channel of Fig. 2 for $Re = 500$ and $Pr = 5$. Curves are drawn every 5% of the difference between the maximum and the minimum normalized temperature.

ber of iteration, a null evaluation was assigned. In this way, the value of $\alpha$ has been found, which ensured a fast convergence of the iterative solution algorithm. The parental velocity distribution and pressure drop between the inlet and the outlet sections were utilized as an initial guess.

Some corrugation profile optimizations have been carried out for $Re$ equal to 100 and 500, and for $Pr$ equal to 1 and 5. Constraints have been imposed on the minimum and maximum values of $F(X)$, the volume of the corrugated wall, and the pressure drop between the inlet and the outlet sections of the channel portion. In particular, to prevent the channel from being too narrow and the corrugated wall from being too thick, the following constraints have been imposed:

$$\max_x f(x) \leq 0.4 \qquad \min_x f(x) \geq 0.1 \tag{35}$$

Moreover, the analysis has been limited to the case where $L$ is equal to 1 and $\gamma$ to 500 (corresponding to the ratio between the thermal conductivities of copper and water).

By imposing no constraint either on the wall volume or on the pressure drop in the channel, it has been found that a wavy wall profile only maximizes $Nu_e$

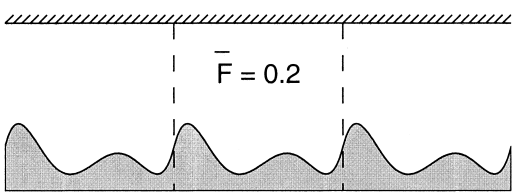


Fig. 5. Optimum channel geometry for $\bar{F}$ constrained to 0.2.

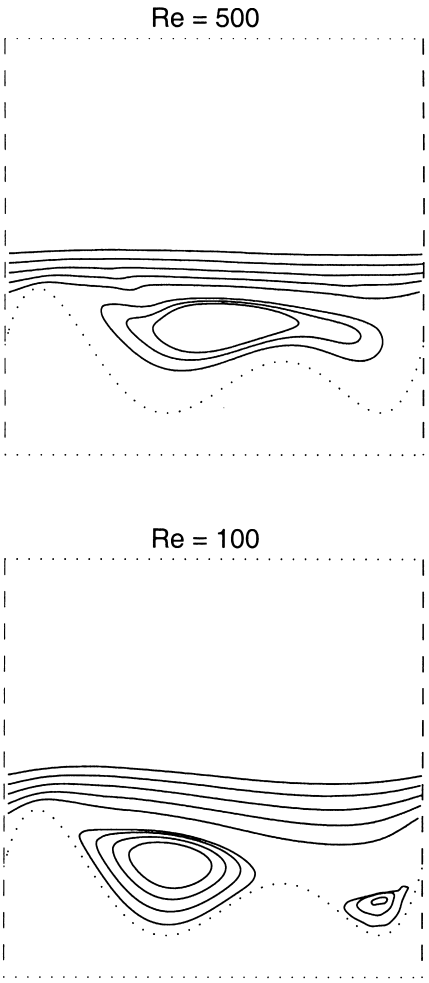


Fig. 6. Streamlines near the corrugated wall of Fig. 5 for $Re$ equal to 100 and 500.

when both $Re$ and $Pr$ are not too low. In particular, for the case where $Re$ is equal to 500 and $Pr$ is equal to 5, the optimum wall profile reported in Fig. 2 has been found. In the other three cases ($Re = 100$ and/or $Pr = 1$), by maximizing $Nu_e$, a flat wall having the maximum allowed thickness has been obtained. The characteristic parameter of the obtained geometries are reported in Table 1, together with those of the geometries discussed in the following. It can be observed that, when $Re$ is equal to 500 and $Pr$ to 5, the wavy wall will provide a 78.6% increment in the heat transfer with respect to the case of a zero thickness wall ($Nu_e = 5.385$) and a 7.6% increment with respect to the case of a maximum thickness wall.

The optimum corrugation profile obtained by maximizing $Nu_e$ for $Re$ equal to 500 and $Pr$ to 5 is composed of two similar wave having the maximum

amplitude. Such a profile coincides with that obtained with the genetic algorithm by maximizing the contact surface between fluid and solid. When *Re* is equal to 500 and *Pr* to 5, the increment of the heat transfer surface between fluid and solid overcome the reductions of the local convective heat transfer coefficient due to the channel enlargements caused by the wavy profile with respect to the case of a maximum thickness wall. On the contrary, when *Re* or *Pr* is lower, such reductions are stronger and cannot be overcome by any extension of the contact surface.

In Figs. 3 and 4 the velocity and temperature distributions in the channel of Fig. 2 are reported for *Re* equal to 500 and *Pr* to 5. One larger eddy occurs in the first cavity and smaller eddies in the second one. Near the peaks the heat is directly transferred from the wall to the main flow due to conduction, so that the isothermal curves are denser. In the cavities, the heat removed from the wall is transferred to the main flow through the eddies. This convective heat transfer mechanism is less efficient when the eddy velocity is lower ($Re = 100$) or the conduction is prevalent ($Pr = 1$), so that, in these cases, the local convection coefficient is noticeably reduced in the cavities.

It is interesting to observe that, for *Re* equal to 500 and *Pr* to 5, the equivalent Nusselt numbers of channels with maximum amplitude sinusolidal corrugation profile having period equal to $l$ and $l/2$ are equal to 8.07 and 8.28, respectively. Therefore, under these conditions, sinusoidal corrugation profiles perform worse than fifth order polynomial and flat profiles.

It must be noticed that the volume of the corrugated

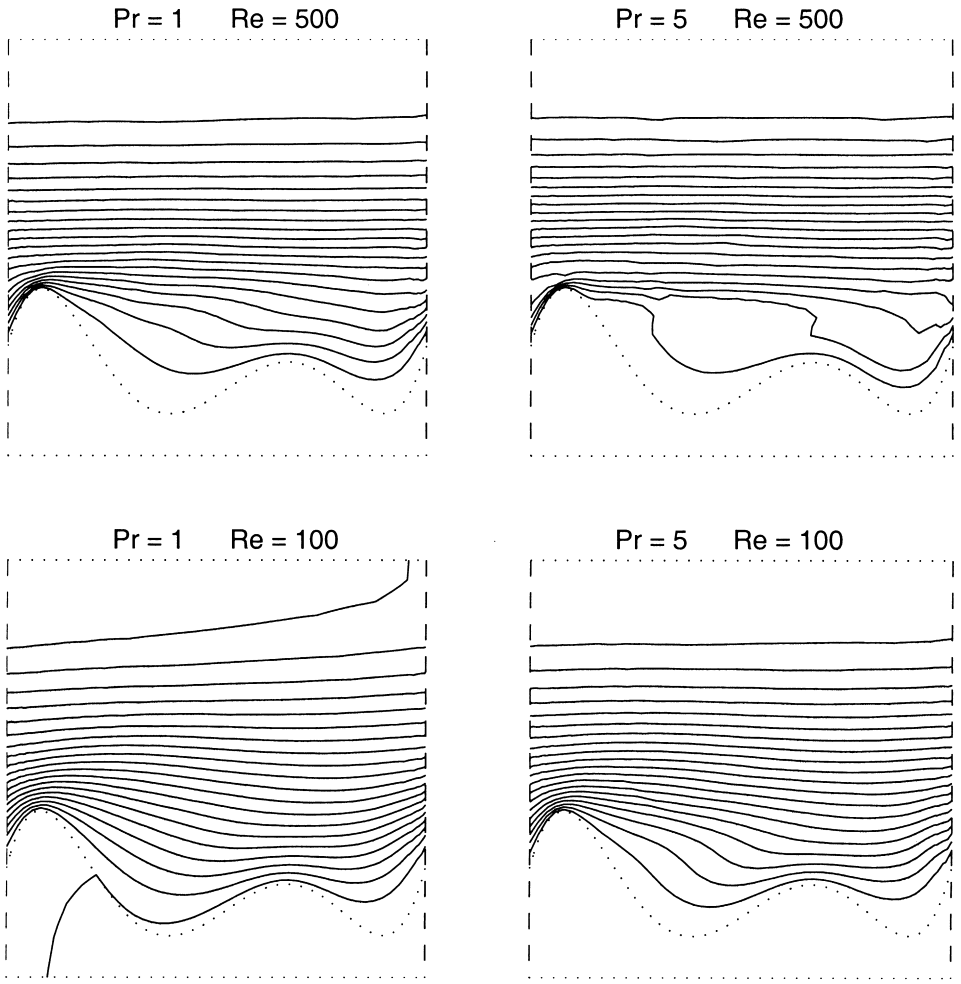


Fig. 7. Isothermal curves in the channel of Fig. 5 for *Re* equal to 100 and 500 and *Pr* equal to 1 and 5. Curves are drawn every 5% of the difference between the maximum and the minimum normalized temperature.

wall of Fig. 2 is much smaller than that of the maximum thickness wall obtained as the optimum one for low Reynolds or Prandtl numbers. If needed, the thickness of the flat wall can be reduced, by decreasing the external size of the channel. In this way, for a given drop between the wall and bulk temperatures, the dissipated heat slightly increases and the system becomes more compact. However, if the external size of the channel is constrained, it can be interesting to optimize the corrugation profile for a given value of the average wall thickness $\bar{F}$, which is representative of the wall volume and weight.

By constraining the volume of the corrugated wall, it has been found that a wavy profile maximizes $Nu_e$ even if $Re$ and/or $Pr$ are low. In particular, by constraining $\bar{F}$ to 0.2, the optimum wall profile reported in Fig. 5 has been obtained in every case. In particular, with respect to the case of a maximum thickness wall ($F(X) = 0.2$; $Nu_e = 6.72$; $\Delta P = 1.95$), the wavy wall of Fig. 5 provides a 30.5% increment in the heat transfer when $Re$ is equal to 500 and $Pr$ to 5, a 8.9% increment when $Re$ is equal to 500 and $Pr$ to 1, and a 7.7% increment when $Re$ is equal to 100 and $Pr$ to 5.

The optimum corrugation profile obtained in every case by maximizing $Nu_e$ for $\bar{F}$ constrained to 0.2 coincides with that obtained with the genetic algorithm by maximizing either the contact surface between fluid and solid or the maximum thickness of the wall. Such a profile provides larger values of the local convection coefficient near the higher peak and a more extended heat transfer surface between fluid and solid with respect to the case of a maximum thickness wall. Therefore, even if the convection in the cavities is reduced for low values of Reynolds or Prandtl numbers, the wavy profile results in being more efficient.

In Figs. 6 and 7 the velocity and temperature distributions in the channel of Fig. 5 are reported. For $Re$ equal to 500, only one larger eddy occurs in the two cavities, while for $Re$ equal to 100 two smaller eddies occur. When $Re$ is lower, for given $q''$, the temperature increment $\Delta t$ is higher, since the mass flow rate is lower. Therefore, the temperature drop between the wall and the fluid is relatively smaller, mainly when $Pr$ is low and the conduction prevails.

By looking at Table 1, it is evident that the corrugated wall of Fig. 5 provides a much larger pressure drop than the flat one having the same volume, while the corrugated wall of Fig. 2 provide a smaller pressure drop than the flat one having the same maximum height. Therefore, it is interesting to find the wall geometry which maximizes $Nu_e$ for a given pressure drop between the inlet and the outlet sections.

By constraining the normalized pressure drop $\Delta P$, it has still been found that a wavy wall profile only maximizes $Nu_e$ when both $Re$ and $Pr$ are not too low. In particular, by constraining $\Delta P$ to 3 and 2.5 the optimum wall profiles reported in Fig. 8 has been found for the case where $Re$ is equal to 500 and $Pr$ to 5. The optimum profiles of Fig. 8 are very similar to that of Fig. 2, but the wave amplitude is reduced. In the other three cases ($Re = 100$ and/or $Pr = 1$), by maximizing $Nu_e$, a flat wall has been obtained having normalized

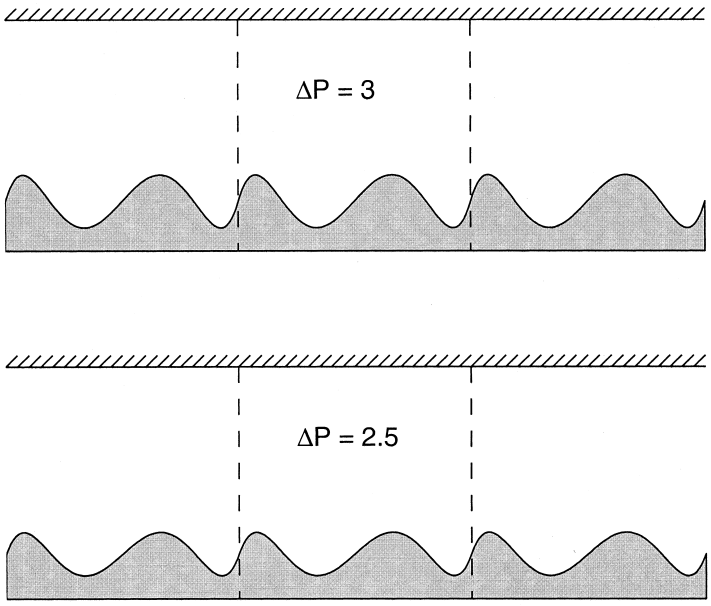


Fig. 8. Optimum channel geometries for $Re = 500$, $Pr = 5$, and $\Delta P$ constrained to 2.5 and 3.

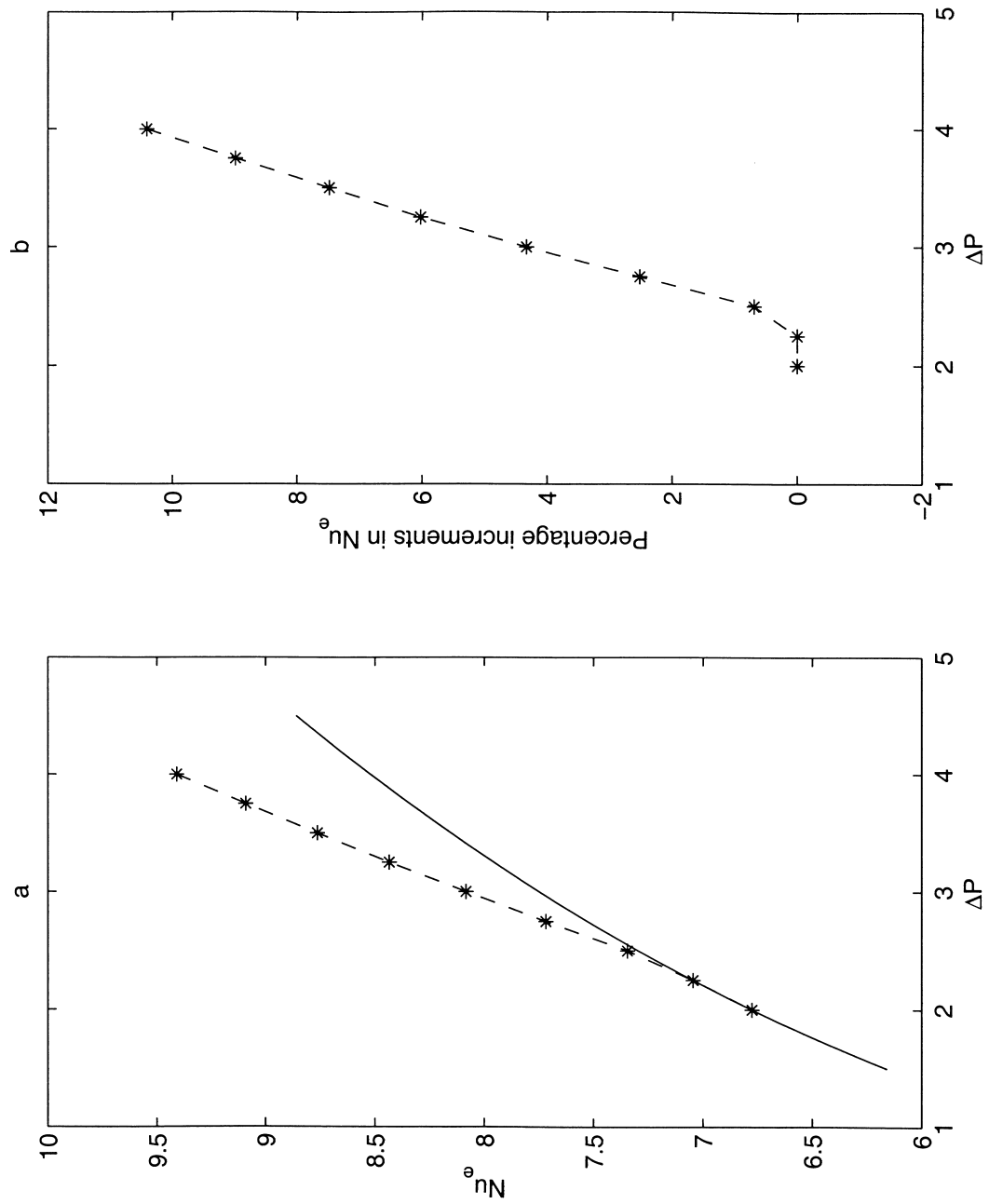


Fig. 9. (a) Comparison between the equivalent Nusselt number analytically calculated for a flat wall channel (continuous line) and the equivalent Nusselt number of the optimum geometries found by the genetic algorithm for $Re = 500$, $Pr = 5$, and $\Delta P$ constrained to different values (stars). (b) Increments in $Nu_e$ of the corrugated channel referred to the value of the flat wall channel.

thickness equal to 0.307 for $\Delta P$ constrained to 3 and to 0.263 for $\Delta P$ constrained to 2.5. However, referring to the heat dissipated through a flat wall causing the same pressure drop, the optimum geometries obtained for the case where $Re$ is equal to 500 and $Pr$ to 5 provide a 4.4% increment when $\Delta P$ is constrained to 3 and only a 0.7% increment when $\Delta P$ is constrained to 2.5. Moreover, by constraining the normalized pressure drop to be less than 2.4, a flat wall has been found to maximize $Nu_e$ even in the case where $Re$ is equal to 500 and $Pr$ to 5 (Fig. 9). Therefore, by assigning to the channel a wavy wall, improvements in the heat transfer can only be obtained when the allowed pressure drop is not too low.

## 4. Conclusions

The proposed mathematical model can be utilized in a genetic algorithm to optimize the geometry of a wall of a plane channel cooled by a laminar flow in order to maximize the heat transferred through the wall. In particular, for a given distance between the external surfaces of the channel, it is possible to determine whether it is more expedient to assign to the wall a corrugated or flat profile, taking some constraints into account on the wall volume or on the pressure drop in the channel.

The results obtained demonstrate that, when no constraint is imposed either on the wall volume or the pressure drop, a corrugated wall profile only maximizes the heat transfer when both the Reynolds and Prandtl numbers are not too low. Under these conditions, in the considered case, the optimum corrugated wall profile found by the genetic algorithm provides a nearly 8% increment with respect to the heat dissipated by the optimum flat wall profile.

Moreover, when both the channel size and the wall volume are constrained, a corrugated wall profile can maximize the heat transfer even if the Reynolds and Prandtl numbers are low. However, the improvements in the heat transfer of the optimum corrugated wall profiles are larger when the Reynolds and Prandtl numbers are higher. In particular, the optimum corrugated wall found by the genetic algorithm provides in the considered cases up to a 30% increment with respect to the heat dissipated by the optimum flat wall of the same volume.

Finally, when the pressure drop in the channel is constrained, a corrugated wall profile can only maximize the heat transfer when the Reynolds and Prandtl numbers and the pressure drop are not too low. For given pressure drop, with respect to the heat dissipated by the optimum flat wall, the optimum corrugated wall profiles found by the genetic algorithm in the considered cases provide up to a 10% increment.

In general, the relative improvements in the heat transfer provided by the optimum fifth order polynomial corrugation profile increase with the Reynolds and Prandtl numbers and with the pressure drop in the channel. Such a result is in accordance with the conclusions of the previous analyses of the heat transfer in corrugated channels considering simpler corrugation profiles such as rectangular [10] or sinusoidal [13]. However, the adoption of a fifth order polynomial profile in the present analysis allows more various and efficient corrugated wall geometries to be considered.

## References

[1] W.M. Kays, A.L. London, Compact Heat Exchangers, 3rd ed., McGraw-Hill, New York, 1984 (Chapter 1).
[2] A. Bar-Cohen, A.D. Kraus, Advances in Thermal Modeling of Electronic Components and Systems, vol. 2, ASME Press Series, New York, 1990, pp. 41–107.
[3] G. Cesini, R. Ricci, B. Ruggeri, Ottimizzazione di dissipatori di calore alettati per applicazioni elettroniche. Modello numerico e verifica sperimentale, in: Proc. 10th UIT National Congress, 1992, pp. 201–212.
[4] L. Goldstein Jr, E.M. Sparrow, Heat/mass characteristics for flow in a corrugated wall channel, ASME J. Heat Transfer 99 (1977) 187–195.
[5] J.E. O' Brien, E.M. Sparrow, Corrugated-duct heat transfer, pressure drop, and flow visualization, ASME J. Heat Transfer 104 (1982) 410–416.
[6] E.M. Sparrow, J.W. Comb, Effect of intervall spacing and fluid flow inlet conditions on a corrugated-wall heat exchanger, Int. J. Heat and Mass Transfer 26 (1983) 993–1004.
[7] K. Ichimiya, Effect of several roughness elements on an insulated wall for heat transfer from the opposite smooth heated surface in a parallel plate duct, ASME J. Heat Transfer 109 (1987) 68–73.
[8] Y. Asako, M. Faghri, Finite-volume solutions for laminar flow and heat transfer in a corrugated duct, ASME J. Heat Transfer 109 (1987) 627–634.
[9] Y. Asako, H. Nakamura, M. Faghri, Heat transfer and pressure drop characteristics in a corrugated duct with rounded corners, Int. J. Heat and Mass Transfer 31 (1988) 1237–1244.
[10] B. Sunden, S. Trollheden, Periodic laminar flow and heat transfer in a corrugated two-dimensional channel, Int. Comm. Heat and Mass Transfer 16 (1989) 215–225.
[11] Q. Xiao, R.C. Xin, W.Q. Tao, Analysis of fully developed laminar flow and heat transfer in asymmetric wavy channels, Int. Comm. Heat and Mass Transfer 16 (1989) 227–236.
[12] S. Blancher, J. Batina, R. Creff, P. Andre, Analysis of convective heat transfer by spectral method for an expanding vortex in a wavy-walled channel, in: Proc. 9th Int. Heat Transfer Conf., vol. 2, Jerusalem, Israel, 1990, pp. 393–401.
[13] G. Tanda, G. Vittori, Studio numerico della convezione forzata in un canale bidimensionale con una parete cor-

rugata, in: Proc. 49th National Congress, Perugia, Italy, 1994, pp. 3–14.
[14] E. Lorenzini, M. Spiga, G. Fabbri, A polynomial fin profile optimization, Int. J. Heat and Technology 12 (1/2) (1994) 137–144.
[15] N. Queipo, R. Devarakonda, J.A.C. Humphrey, Genetic algorithms for thermosciences research: application to the optimized cooling of electronic components, Int. J. Heat and Mass Transfer 37 (6) (1994) 893–908.
[16] G. Fabbri, A genetic algorithm for fin profile optimization, Int. J. Heat and Mass Transfer 40 (9) (1997) 2165–2172.
[17] G. Fabbri, Heat transfer optimization in internally finned tubes under laminar flow conditions, Int. J. Heat and Mass Transfer 41 (10) (1998) 1243–1253.
[18] G. Fabbri, Optimum profiles for asymmetrical longitudinal fins in cylindrical ducts, Int. J. of Heat and Mass Transfer 42 (3) (1999) 511–523.